

Single Spin Asymmetry A_N in Polarized Proton-Proton Elastic Scattering at $\sqrt{s} = 200$ GeV

L. Adamczyk,¹ G. Agakishiev,²¹ M. M. Aggarwal,³⁴ Z. Ahammed,⁵³ A. V. Alakhverdyants,²¹ I. Alekseev,¹⁹ J. Alford,²² C. D. Anson,³¹ D. Arkhipkin,⁴ E. Aschenauer,⁴ G. S. Averichev,²¹ J. Balewski,²⁶ A. Banerjee,⁵³ Z. Barnovska,¹⁴ D. R. Beavis,⁴ R. Bellwied,⁴⁹ M. J. Betancourt,²⁶ R. R. Betts,¹⁰ A. Bhasin,²⁰ A. K. Bhati,³⁴ H. Bichsel,⁵⁵ J. Bielcik,¹³ J. Bielcikova,¹⁴ L. C. Bland,⁴ I. G. Bordyuzhin,¹⁹ W. Borowski,⁴⁵ J. Bouchet,²² A. V. Brandin,²⁹ S. G. Brovko,⁶ E. Bruna,⁵⁷ S. Bültmann,³² I. Bunzarov,²¹ T. P. Burton,⁴ J. Butterworth,⁴⁰ X. Z. Cai,⁴⁴ H. Caines,⁵⁷ M. Calderón de la Barca Sánchez,⁶ D. Cebra,⁶ R. Cendejas,⁷ M. C. Cervantes,⁴⁷ P. Chaloupka,¹³ Z. Chang,⁴⁷ S. Chattopadhyay,⁵³ H. F. Chen,⁴² J. H. Chen,⁴⁴ J. Y. Chen,⁹ L. Chen,⁹ J. Cheng,⁵⁰ M. Cherney,¹² A. Chikanian,⁵⁷ W. Christie,⁴ P. Chung,¹⁴ J. Chwastowski,¹¹ M. J. M. Codrington,⁴⁷ R. Corliss,²⁶ J. G. Cramer,⁵⁵ H. J. Crawford,⁵ X. Cui,⁴² S. Das,¹⁶ A. Davila Leyva,⁴⁸ L. C. De Silva,⁴⁹ R. R. Debbe,⁴ T. G. Dedovich,²¹ J. Deng,⁴³ R. Derradi de Souza,⁸ S. Dhamija,¹⁸ L. Didenko,⁴ F. Ding,⁶ A. Dion,⁴ P. Djawotho,⁴⁷ X. Dong,²⁵ J. L. Drachenberg,⁴⁷ J. E. Draper,⁶ C. M. Du,²⁴ L. E. Dunkelberger,⁷ J. C. Dunlop,⁴ L. G. Efimov,²¹ M. Elnimr,⁵⁶ J. Engelage,⁵ G. Eppley,⁴⁰ L. Eun,²⁵ O. Evdokimov,¹⁰ R. Fatemi,²³ S. Fazio,⁴ J. Fedorisin,²¹ R. G. Fersch,²³ P. Filip,²¹ E. Finch,⁵⁷ Y. Fisyak,⁴ C. A. Gagliardi,⁴⁷ D. R. Gangadharan,³¹ F. Geurts,⁴⁰ A. Gibson,⁵² S. Gliske,² Y. N. Gorbunov,¹² O. G. Grebenyuk,²⁵ D. Grosnick,⁵² S. Gupta,²⁰ W. Guryn,⁴ B. Haag,⁶ O. Hajkova,¹³ A. Hamed,⁴⁷ L.-X. Han,⁴⁴ J. W. Harris,⁵⁷ J. P. Hays-Wehle,²⁶ S. Heppelmann,³⁵ A. Hirsch,³⁷ G. W. Hoffmann,⁴⁸ D. J. Hofman,¹⁰ S. Horvat,⁵⁷ B. Huang,⁴ H. Z. Huang,⁷ P. Huck,⁹ T. J. Humanic,³¹ L. Huo,⁴⁷ G. Igo,⁷ W. W. Jacobs,¹⁸ C. Jena,³⁰ E. G. Judd,⁵ S. Kabana,⁴⁵ K. Kang,⁵⁰ J. Kapitan,¹⁴ K. Kauder,¹⁰ H. W. Ke,⁹ D. Keane,²² A. Kechechyan,²¹ A. Kesich,⁶ D. P. Kikola,³⁷ J. Kiryluk,²⁵ I. Kisel,²⁵ A. Kisiel,⁵⁴ V. Kizka,²¹ S. R. Klein,²⁵ D. D. Koetke,⁵² T. Kollegger,¹⁵ J. Konzer,³⁷ I. Koralt,³² L. Koroleva,¹⁹ W. Korsch,²³ L. Kotchenda,²⁹ P. Kravtsov,²⁹ K. Krueger,² I. Kulakov,²⁵ L. Kumar,²² M. A. C. Lamont,⁴ J. M. Landgraf,⁴ S. LaPointe,⁵⁶ J. Lauret,⁴ A. Lebedev,⁴ R. Lednicky,²¹ J. H. Lee,⁴ W. Leight,²⁶ M. J. LeVine,⁴ C. Li,⁴² L. Li,⁴⁸ W. Li,⁴⁴ X. Li,³⁷ X. Li,⁴⁶ Y. Li,⁵⁰ Z. M. Li,⁹ L. M. Lima,⁴¹ M. A. Lisa,³¹ F. Liu,⁹ T. Ljubicic,⁴ W. J. Llope,⁴⁰ R. S. Longacre,⁴ Y. Lu,⁴² X. Luo,⁹ A. Luszczak,¹¹ G. L. Ma,⁴⁴ Y. G. Ma,⁴⁴ D. M. M. D. Madagadage, Don,¹² D. P. Mahapatra,¹⁶ R. Majka,⁵⁷ O. I. Mall,⁶ S. Margetis,²² C. Markert,⁴⁸ H. Masui,²⁵ H. S. Matis,²⁵ D. McDonald,⁴⁰ T. S. McShane,¹² S. Mioduszewski,⁴⁷ M. K. Mitrovski,⁴ Y. Mohammed,⁴⁷ B. Mohanty,³⁰ M. M. Mondal,⁴⁷ B. Morozov,¹⁹ M. G. Munhoz,⁴¹ M. K. Mustafa,³⁷ M. Naglis,²⁵ B. K. Nandi,¹⁷ Md. Nasim,⁵³ T. K. Nayak,⁵³ J. M. Nelson,³ L. V. Nogach,³⁶ J. Novak,²⁸ G. Odyniec,²⁵ A. Ogawa,⁴ K. Oh,³⁸ A. Ohlson,⁵⁷ V. Okorokov,²⁹ E. W. Oldag,⁴⁸ R. A. N. Oliveira,⁴¹ D. Olson,²⁵ P. Ostrowski,⁵⁴ M. Pachr,¹³ B. S. Page,¹⁸ S. K. Pal,⁵³ Y. X. Pan,⁷ Y. Pandit,²² Y. Panebratsev,²¹ T. Pawlak,⁵⁴ B. Pawlik,³³ H. Pei,¹⁰ C. Perkins,⁵ W. Peryt,⁵⁴ P. Pile,⁴ M. Planinic,⁵⁸ J. Pluta,⁵⁴ D. Plyku,³² N. Poljak,⁵⁸ J. Porter,²⁵ A. M. Poskanzer,²⁵ C. B. Powell,²⁵ C. Pruneau,⁵⁶ N. K. Pruthi,³⁴ M. Przybycien,¹ P. R. Pujahari,¹⁷ J. Putschke,⁵⁶ H. Qiu,²⁵ R. Raniwala,³⁹ S. Raniwala,³⁹ R. L. Ray,⁴⁸ R. Redwine,²⁶ R. Reed,⁶ C. K. Riley,⁵⁷ H. G. Ritter,²⁵ J. B. Roberts,⁴⁰ O. V. Rogachevskiy,²¹ J. L. Romero,⁶ J. F. Ross,¹² L. Ruan,⁴ J. Rusnak,¹⁴ N. R. Sahoo,⁵³ P. K. Sahu,¹⁶ I. Sakrejda,²⁵ S. Salur,²⁵ A. Sandacz,⁵⁴ J. Sandweiss,⁵⁷ E. Sangaline,⁶ A. Sarkar,¹⁷ J. Schambach,⁴⁸ R. P. Scharenberg,³⁷ A. M. Schmah,²⁵ B. Schmidke,⁴ N. Schmitz,²⁷ T. R. Schuster,¹⁵ J. Seele,²⁶ J. Seger,¹² P. Seyboth,²⁷ N. Shah,⁷ E. Shahaliev,²¹ M. Shao,⁴² B. Sharma,³⁴ M. Sharma,⁵⁶ S. S. Shi,⁹ Q. Y. Shou,⁴⁴ E. P. Sichtermann,²⁵ R. N. Singaraju,⁵³ M. J. Skoby,¹⁸ D. Smirnov,⁴ N. Smirnov,⁵⁷ D. Solanki,³⁹ P. Sorensen,⁴ U. G. deSouza,⁴¹ H. M. Spinka,² B. Srivastava,³⁷ T. D. S. Stanislaus,⁵² S. G. Steadman,²⁶ J. R. Stevens,¹⁸ R. Stock,¹⁵ M. Strikhanov,²⁹ B. Stringfellow,³⁷ A. A. P. Suaide,⁴¹ M. C. Suarez,¹⁰ M. Sumbera,¹⁴ X. M. Sun,²⁵ Y. Sun,⁴² Z. Sun,²⁴ B. Surrus,⁴⁶ D. N. Svirida,¹⁹ T. J. M. Symons,²⁵ A. Szanto de Toledo,⁴¹ J. Takahashi,⁸ A. H. Tang,⁴ Z. Tang,⁴² L. H. Tarini,⁵⁶ T. Tarnowsky,²⁸ D. Thein,⁴⁸ J. H. Thomas,²⁵ J. Tian,⁴⁴ A. R. Timmins,⁴⁹ D. Tlusty,¹⁴ M. Tokarev,²¹ S. Trentalange,⁷ R. E. Tribble,⁴⁷ P. Tribedy,⁵³ B. A. Trzeciak,⁵⁴ O. D. Tsai,⁷ J. Turnau,³³ T. Ullrich,⁴ D. G. Underwood,² G. Van Buren,⁴ G. van Nieuwenhuizen,²⁶ J. A. Vanfossen, Jr.,²² R. Varma,¹⁷ G. M. S. Vasconcelos,⁸ F. Videbæk,⁴ Y. P. Viyogi,⁵³ S. Vokal,²¹ S. A. Voloshin,⁵⁶ A. Vossen,¹⁸ M. Wada,⁴⁸ F. Wang,³⁷ G. Wang,⁷ H. Wang,⁴ J. S. Wang,²⁴ Q. Wang,³⁷ X. L. Wang,⁴² Y. Wang,⁵⁰ G. Webb,²³ J. C. Webb,⁴ G. D. Westfall,²⁸ C. Whitten Jr.,⁷ H. Wieman,²⁵ S. W. Wissink,¹⁸ R. Witt,⁵¹ W. Witzke,²³ Y. F. Wu,⁹ Z. Xiao,⁵⁰ W. Xie,³⁷ K. Xin,⁴⁰ H. Xu,²⁴ N. Xu,²⁵ Q. H. Xu,⁴³ W. Xu,⁷ Y. Xu,⁴² Z. Xu,⁴ L. Xue,⁴⁴ Y. Yang,²⁴ Y. Yang,⁹ P. Yepes,⁴⁰ Y. Yi,³⁷ K. Yip,⁴ I.-K. Yoo,³⁸ M. Zawisza,⁵⁴ H. Zbroszczyk,⁵⁴ J. B. Zhang,⁹ S. Zhang,⁴⁴ X. P. Zhang,⁵⁰ Y. Zhang,⁴² Z. P. Zhang,⁴² F. Zhao,⁷ J. Zhao,⁴⁴ C. Zhong,⁴⁴ X. Zhu,⁵⁰ Y. H. Zhu,⁴⁴ Y. Zoukarneeva,²¹ and M. Zyzak²⁵

(STAR Collaboration)

- ¹AGH University of Science and Technology, Cracow, Poland
²Argonne National Laboratory, Argonne, Illinois 60439, USA
³University of Birmingham, Birmingham, United Kingdom
⁴Brookhaven National Laboratory, Upton, New York 11973, USA
⁵University of California, Berkeley, California 94720, USA
⁶University of California, Davis, California 95616, USA
⁷University of California, Los Angeles, California 90095, USA
⁸Universidade Estadual de Campinas, Sao Paulo, Brazil
⁹Central China Normal University (HZNU), Wuhan 430079, China
¹⁰University of Illinois at Chicago, Chicago, Illinois 60607, USA
¹¹Cracow University of Technology, Cracow, Poland
¹²Creighton University, Omaha, Nebraska 68178, USA
¹³Czech Technical University in Prague, FNSPE, Prague, 115 19, Czech Republic
¹⁴Nuclear Physics Institute AS CR, 250 68 Řež/Prague, Czech Republic
¹⁵University of Frankfurt, Frankfurt, Germany
¹⁶Institute of Physics, Bhubaneswar 751005, India
¹⁷Indian Institute of Technology, Mumbai, India
¹⁸Indiana University, Bloomington, Indiana 47408, USA
¹⁹Alikhanov Institute for Theoretical and Experimental Physics, Moscow, Russia
²⁰University of Jammu, Jammu 180001, India
²¹Joint Institute for Nuclear Research, Dubna, 141 980, Russia
²²Kent State University, Kent, Ohio 44242, USA
²³University of Kentucky, Lexington, Kentucky, 40506-0055, USA
²⁴Institute of Modern Physics, Lanzhou, China
²⁵Lawrence Berkeley National Laboratory, Berkeley, California 94720, USA
²⁶Massachusetts Institute of Technology, Cambridge, MA 02139-4307, USA
²⁷Max-Planck-Institut für Physik, Munich, Germany
²⁸Michigan State University, East Lansing, Michigan 48824, USA
²⁹Moscow Engineering Physics Institute, Moscow Russia
³⁰National Institute of Science and Education and Research, Bhubaneswar 751005, India
³¹Ohio State University, Columbus, Ohio 43210, USA
³²Old Dominion University, Norfolk, VA, 23529, USA
³³Institute of Nuclear Physics PAN, Cracow, Poland
³⁴Panjab University, Chandigarh 160014, India
³⁵Pennsylvania State University, University Park, Pennsylvania 16802, USA
³⁶Institute of High Energy Physics, Protvino, Russia
³⁷Purdue University, West Lafayette, Indiana 47907, USA
³⁸Pusan National University, Pusan, Republic of Korea
³⁹University of Rajasthan, Jaipur 302004, India
⁴⁰Rice University, Houston, Texas 77251, USA
⁴¹Universidade de Sao Paulo, Sao Paulo, Brazil
⁴²University of Science & Technology of China, Hefei 230026, China
⁴³Shandong University, Jinan, Shandong 250100, China
⁴⁴Shanghai Institute of Applied Physics, Shanghai 201800, China
⁴⁵SUBATECH, Nantes, France
⁴⁶Temple University, Philadelphia, Pennsylvania, 19122
⁴⁷Texas A&M University, College Station, Texas 77843, USA
⁴⁸University of Texas, Austin, Texas 78712, USA
⁴⁹University of Houston, Houston, TX, 77204, USA
⁵⁰Tsinghua University, Beijing 100084, China
⁵¹United States Naval Academy, Annapolis, MD 21402, USA
⁵²Valparaiso University, Valparaiso, Indiana 46383, USA
⁵³Variable Energy Cyclotron Centre, Kolkata 700064, India
⁵⁴Warsaw University of Technology, Warsaw, Poland
⁵⁵University of Washington, Seattle, Washington 98195, USA
⁵⁶Wayne State University, Detroit, Michigan 48201, USA
⁵⁷Yale University, New Haven, Connecticut 06520, USA
⁵⁸University of Zagreb, Zagreb, HR-10002, Croatia

We report a high precision measurement of the transverse single spin asymmetry A_N at the center of mass energy $\sqrt{s} = 200$ GeV in elastic proton-proton scattering by the STAR experiment at RHIC. The A_N was measured in the four-momentum transfer squared t range $0.003 \leq |t| \leq 0.035$ (GeV/c)², the region of a significant interference between the electromagnetic and hadronic scattering amplitudes. The measured values of A_N and its t -dependence are consistent with a

vanishing hadronic spin-flip amplitude, thus providing strong constraints on the ratio of the single spin-flip to the non-flip amplitudes. Since the hadronic amplitude is dominated by the Pomeron amplitude at this \sqrt{s} , we conclude that this measurement addresses the question about the presence of a hadronic spin flip due to the Pomeron exchange in polarized proton-proton elastic scattering.

PACS numbers: 13.85.Dz and 13.88.+e

I. INTRODUCTION

High energy diffractive hadronic scattering at small values of four-momentum transfer squared t , is dominated by an exchange of the Pomeron trajectory, a color-singlet object with the quantum numbers of the vacuum [1, 2]. The calculation of cross-sections for small- t scattering requires a non-perturbative approach in QCD and its theoretical treatment is still being developed. The experimental data therefore provide significant constraints for theoretical approaches and models [3, 4]. The coupling of the Pomeron to the nucleon spin is of special interest since it is predicted to be sensitive to the internal dynamics of the nucleon [3, 4]. Studies of the spin dependence of proton-proton (pp) scattering at small momentum transfers and at the highest energies presently available at RHIC offer an opportunity to reveal important information on the nature of the Pomeron.

There are several theoretical approaches which predict non-zero spin-dependent Pomeron amplitudes for elastic scattering. Examples include an approach in which the Pomeron-proton coupling is modeled via two-pion exchange [5], an impact picture model assuming that the spin-flip contribution is sensitive to the impact parameter distribution of matter in a polarized proton [6], and a model which treats the Pomeron helicity coupling analogously to that of the isoscalar anomalous magnetic moment of the nucleon [7]. Still another approach assumes a diquark enhanced picture of the proton [8], in which a non-zero spin-flip amplitude may arise if the proton wave function is dominated by an asymmetric configuration, such as a quark-diquark.

Here we present a high precision measurement of the transverse single spin asymmetry A_N in elastic scattering of polarized protons at $\sqrt{s} = 200$ GeV in the t -range $0.003 \leq |t| \leq 0.035$ (GeV/ c)² by the STAR experiment [9] at RHIC. The single spin asymmetry A_N is defined as the left-right cross-section asymmetry with respect to the transversely polarized proton beam. In this range of t , A_N originates predominantly from the interference between electromagnetic (Coulomb) spin-flip and hadronic (nuclear) non-flip amplitudes [3]. However, it was realized that A_N in the Coulomb-nuclear interference (CNI) region is also a sensitive probe of the hadronic spin-flip amplitude [8], which will be discussed in more detail in Section II.

A previous measurement of A_N in a similar t -range and the same \sqrt{s} , but with limited statistics, has been reported by the pp2pp collaboration [10]. Other measurements of A_N performed at small t were obtained at significantly lower energies. They include high precision results from the RHIC polarimeters obtained at $\sqrt{s} = 6.8 - 21.7$ GeV for elastic proton-proton [11–13] and proton-carbon [14] scattering, as well as earlier results from the BNL AGS for pC scattering [15] at $\sqrt{s} = 6.4$ GeV and from FNAL E704 for pp scattering [16] at $\sqrt{s} = 19.4$ GeV.

The combined analysis of all results, which covers a wide energy range and different targets, will help to disentangle contributions of various exchange mechanisms relevant for elastic scattering in the forward region [17]. In particular, such an analysis will allow us to extract information on the spin dependence of the diffractive mechanism which dominates at high energies.

II. HADRONIC SPIN-FLIP AMPLITUDE IN ELASTIC COLLISIONS

Elastic scattering of two protons is described by five independent helicity amplitudes: two helicity conserving (ϕ_1 and ϕ_3), two double helicity-flip (ϕ_2 and ϕ_4), and one single helicity-flip amplitude (ϕ_5) – see [3] for definitions. At very high \sqrt{s} , such as available at RHIC, and very small $|t| < 0.05$ (GeV/ c)², the proton mass m can be neglected with respect to \sqrt{s} and t can be neglected with respect to m , which simplifies kinematical factors in the following formulas. The elastic spin-averaged cross-section is given by:

$$\frac{d\sigma}{dt} = \frac{2\pi}{s^2} (|\phi_1|^2 + |\phi_2|^2 + |\phi_3|^2 + |\phi_4|^2 + 4|\phi_5|^2), \quad (1)$$

while the single spin-flip amplitude ϕ_5 gives rise to the single spin asymmetry, A_N , through interference with the remaining amplitudes:

$$A_N \frac{d\sigma}{dt} = -\frac{4\pi}{s^2} \text{Im} \{ \phi_5^* (\phi_1 + \phi_2 + \phi_3 - \phi_4) \}. \quad (2)$$

Each of the amplitudes consists of Coulomb and hadronic contributions: $\phi_i = \phi_i^{\text{em}} + \phi_i^{\text{had}}$, with the electromagnetic one-photon exchange amplitudes ϕ_i^{em} described by QED using the measured anomalous magnetic moment of the proton. [18]. The optical theorem relates the hadronic amplitudes to the total cross-section:

$$\sigma_{\text{total}} = \frac{4\pi}{s} \text{Im} (\phi_1^{\text{had}} + \phi_3^{\text{had}})|_{t=0}, \quad (3)$$

which provides an important constraint on the parameterization of these dominant helicity conserving hadronic amplitudes.

The contribution of the two double spin-flip hadronic amplitudes ϕ_2^{had} and ϕ_4^{had} to the asymmetry A_N is small, as indicated by both experimental results [19, 20] and theoretical predictions [21]. Thus, the main contribution to A_N is given by:

$$A_N \frac{d\sigma}{dt} = -\frac{8\pi}{s^2} \text{Im} (\phi_5^{\text{em}*} \phi_+^{\text{had}} + \phi_5^{\text{had}*} \phi_+^{\text{em}}), \quad (4)$$

where $\phi_+ = (\phi_1 + \phi_3)/2$.

The parametrization of ϕ_5^{had} is usually done in terms of ϕ_+^{had} : $\phi_5^{\text{had}}(s, t) = (\sqrt{-t}/m) \cdot r_5(s) \cdot \text{Im} \phi_+^{\text{had}}(s, t)$, where m is the proton mass. Thus r_5 is the measure of the ratio of the hadronic single spin-flip amplitude (ϕ_5) to hadronic single non-flip amplitudes (ϕ_1 and ϕ_3). Using this parametrization the following representation of A_N can be derived [3]:

$$A_N = \frac{\sqrt{-t}}{m} \frac{[\kappa(1 - \rho \delta) + 2(\delta \text{Re } r_5 - \text{Im } r_5)] \frac{t_c}{t} - 2(\text{Re } r_5 - \rho \text{Im } r_5)}{(\frac{t_c}{t})^2 - 2(\rho + \delta) \frac{t_c}{t} + (1 + \rho^2)}, \quad (5)$$

where $t_c = -8\pi\alpha/\sigma_{\text{total}}$, κ is the anomalous magnetic moment of the proton, $\rho = \text{Re } \phi_+ / \text{Im } \phi_+$ is the ratio of the real to imaginary parts of the non-flip elastic amplitude, and δ is the relative phase between the Coulomb and hadronic amplitudes [3]:

$$\delta = \alpha \ln \frac{2}{|t|(B + 8/\Lambda^2)} - \alpha \gamma, \quad (6)$$

where B is the slope of the forward peak in elastic scattering, $\alpha = 1/137$ is the fine structure constant, $\gamma = 0.5772$ is Euler's constant, and $\Lambda^2 = 0.71$ (GeV/c)².

III. DETECTION OF ELASTIC PROTON-PROTON COLLISIONS AT RHIC

The protons, which scatter elastically at small angles ($\lesssim 2$ mrad), follow the optics of the RHIC magnets and are detected by a system of detectors placed close to the beam inside movable vessels known as ‘‘Roman Pots’’ (RPs) [22]. The Roman Pot stations are located on either side of the STAR interaction point (IP) at 55.5 m and 58.5 m with horizontal and vertical insertions of the detectors, respectively. The coordinate system of the experiment is described in Fig. 1. There are eight Roman Pots, four on each side of the IP. Four approach the beam horizontally WHI, WHO (EHI, EHO) and four approach the beam vertically WVU, WVD (EVU, EVD) as shown in Fig. 1. The location of the RPs was optimized so that, combined with proper accelerator magnet settings, it provides so-called ‘‘parallel-to-point focusing’’, i.e. the (x, y) position of the scattered protons at the RPs depends almost exclusively on their scattering angles and is nearly insensitive to the transverse position of the interaction point. As shown in Fig. 1, there are five major magnets between the RPs and the collision point, two dipole magnets DX and D0, which bend beams into collision, and the focusing triplet of quadrupoles Q1-Q3. The dipole magnets scatter out particles with momentum which is not close to the beam momentum. The detector package inside each RP consists of four 0.4 mm thick silicon micro-strip detector planes with a strip pitch of about 100 μm , two of them measuring the horizontal (x) and two the vertical (y) position of a scattered proton. The sensitive area of the detectors is 79×48 mm². Scintillation counters covering this area are used to form a trigger for elastic events. More details on the experiment and the technique can be found in Refs. [22, 23].

The preliminary alignment was done by surveying the detector packages during their assembly and after installation inside the Roman Pots with respect to the beam line of the accelerator. The displacement of the RPs during data taking was measured by linear variable differential transformers (LVDTs). The final alignment was done using elastic events in the overlapping regions of horizontal and vertical RPs, which allowed a relative position measurement of the RPs on each side of the IP with a precision better than 0.1 mm. Collinearity of the elastic events and Monte-Carlo

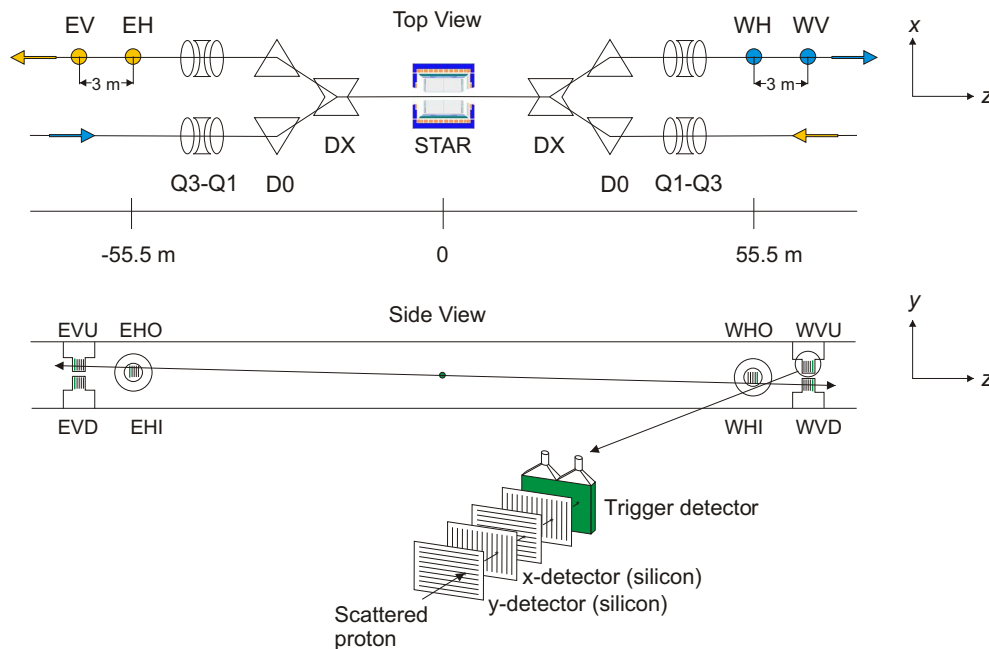


FIG. 1: (color online) The layout of the experiment. The Roman Pot stations are located on both sides of the STAR IP. The positive z direction is defined along the outgoing “Blue” beam (the West direction). Positive y is pointing up and positive x is pointing away from the center of the RHIC ring. The detectors are placed on the outgoing beams. The figure is not to scale.

simulations of the acceptance boundaries due to limiting apertures in the quadrupole magnets were used to further constrain the geometry and to estimate systematic errors.

The data were taken during four dedicated RHIC stores between June 30 and July 4, 2009 with special beam optics of $\beta^* = 22$ m in order to minimize the angular divergence at the IP [24]. The average luminosity over the four stores during which the data were collected was $\mathcal{L} \approx 2 \cdot 10^{29} \text{cm}^{-2} \text{s}^{-1}$. The closest approach of the first strip to the center of the beam was about 10 mm or about 12σ of the transverse beam size. A total of 33 million elastic triggers were recorded.

IV. DATA SELECTION AND RECONSTRUCTION OF ELASTIC SCATTERING EVENTS

The selection of elastic events in this experiment is based on the collinearity of the scattered proton tracks. A single track was required on each side of the IP. Noisy and dead strips were rejected, with a total of five out of $\approx 14,000$ in the active detector area. Track reconstruction started with the search for hits in the silicon detectors. First, adjacent strips with collected charge values above 5σ from their pedestal averages were found and combined into clusters. A threshold depending on the cluster width was applied to the total charge of the cluster, thus improving the signal-to-noise ratio for clusters of 3 to 5 strips, while wider clusters were rejected. The cluster position was determined as a charge weighted average of strip coordinates. For each RP a search was performed for matching clusters in the pairs of planes measuring the same coordinate. Two clusters in such planes were considered matched if the distance between them was smaller than $200 \mu\text{m}$, approximately the width of two strips. A matching pair with the smallest matching distance was chosen and its cluster coordinates were averaged. If only one cluster in the pair of planes was found, we just use its coordinate for the analysis. If more than one cluster or no match was found, no output from this RP was selected. An (x, y) pair found in an RP was considered a track. About 1/3 of all reconstructed tracks were found in the region of overlapping acceptance between the horizontal and the vertical RPs; for those tracks the average of the kinematic variables was used. To minimize the background contribution from beam halo particles, products of beam-gas interactions, and detector noise, fiducial areas were selected to cut edges of the silicon detectors near the beam and boundaries of the magnet apertures.

Planar angles θ_x^{RP} , θ_y^{RP} and coordinates x^{RP} , y^{RP} of protons at a given RP relate to the angles θ_x , θ_y and coordinates

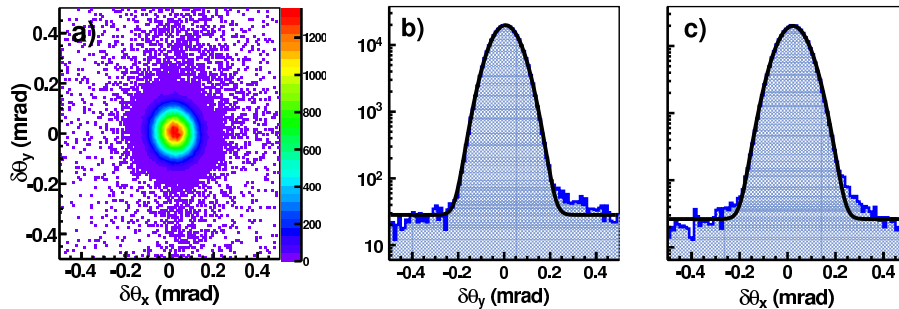


FIG. 2: (color online) Distribution of $\delta\theta_y$ vs. $\delta\theta_x$ for both detector pairs in horizontal RPs (a) and their projections in $\delta\theta_y$ (b) and $\delta\theta_x$ (c). The overlaid curves represent the fits with a Gaussian signal and a linear background. The σ values of distributions are $\approx 58 \mu\text{rad}$, consistent with beam angular divergence, and the background-to-signal ratio under the Gaussian distributions in $\pm 3 \sigma$ is $\approx 0.4\%$.

x, y at the IP by the transport matrix \mathbf{M} :

$$\begin{bmatrix} x^{\text{RP}} \\ \theta_x^{\text{RP}} \\ y^{\text{RP}} \\ \theta_y^{\text{RP}} \end{bmatrix} = \mathbf{M} \begin{bmatrix} x \\ \theta_x \\ y \\ \theta_y \end{bmatrix} = \begin{bmatrix} a_{11} & L_x^{\text{eff}} & a_{13} & a_{14} \\ a_{21} & a_{22} & a_{23} & a_{24} \\ a_{31} & a_{32} & a_{33} & L_y^{\text{eff}} \\ a_{41} & a_{42} & a_{43} & a_{44} \end{bmatrix} \begin{bmatrix} x \\ \theta_x \\ y \\ \theta_y \end{bmatrix}. \quad (7)$$

For example, the transport matrix \mathbf{M} for the horizontal Roman Pot in the West side of the IP (WHI,WHO) is:

$$\mathbf{M} = \begin{bmatrix} -0.0913 & 25.2566 \text{ m} & -0.0034 & 0.0765 \text{ m} \\ -0.0396 \text{ m}^{-1} & 0.0137 & -0.0001 \text{ m}^{-1} & 0.0057 \\ -0.0033 & -0.1001 \text{ m} & 0.1044 & 24.7598 \text{ m} \\ 0.0002 \text{ m}^{-1} & 0.0083 & -0.0431 \text{ m}^{-1} & -0.6332 \end{bmatrix}.$$

For the case of parallel-to-point focusing, and in the absence of x - y mixing, the transport matrix is simplified and the so-called “effective” length, L^{eff} , terms dominate. The L^{eff} values are in the range of 22-26 m for this experiment. The angles of the scattered protons at the IP can then be reconstructed independently for the East (E) and West (W) arms with respect to the IP:

$$\theta_x = x^{\text{RP}} / L_x^{\text{eff}}, \quad (8)$$

$$\theta_y = y^{\text{RP}} / L_y^{\text{eff}}. \quad (9)$$

Because non-dominant terms in the transport matrix are small and result in a negligible correction of about $4 \mu\text{rad}$ to the reconstruction of the scattering angles, we used a 2×2 matrix ($L_x^{\text{eff}}, a_{14}; a_{32}, L_y^{\text{eff}}$), which was obtained by neglecting those small terms of the transport matrix.

Once the planar angles at IP were reconstructed, a collinearity requirement was imposed using χ^2 defined as:

$$\chi^2 = [(\delta\theta_x - \bar{\delta\theta}_x) / \sigma_{\theta_x}]^2 + [(\delta\theta_y - \bar{\delta\theta}_y) / \sigma_{\theta_y}]^2, \quad (10)$$

where $\delta\theta_{x,y} = [\theta_{x,y}^W - \theta_{x,y}^E]$ and the mean values $\bar{\delta\theta}_{x,y}$ and widths $\sigma_{\theta_{x,y}}$ are taken from the fits to data performed for each data sample. An example is shown in Fig. 2. The small non-zero mean values ($\approx 10 \mu\text{rad}$) are consistent with the uncertainties of angle determinations discussed in the next section. Fig. 2 shows a typical distribution of $\delta\theta_y$ vs. $\delta\theta_x$ and its projections, fitted with a Gaussian and a linear background. Based on these fits, the non-collinear background contribution is estimated to be 0.3-0.5%. The requirement of $\chi^2 < 9$ left about 21 million events for the asymmetry calculations.

The polar scattering angle θ and azimuthal angle φ (measured counterclockwise from the positive x-axis) for an event were then calculated as an average of those obtained from East and West arms, and the four-momentum transfer squared, t , was assigned to the event using $t = -2p^2(1 - \cos\theta) \approx -p^2\theta^2$ with $p = 100.2 \text{ GeV}/c$.

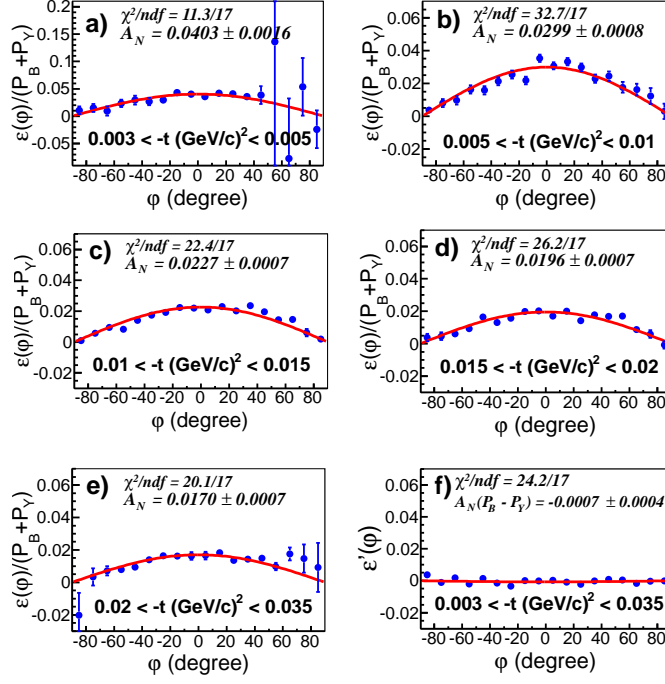


FIG. 3: (color online) The asymmetry $\varepsilon(\varphi)/(\mathcal{P}_B + \mathcal{P}_Y)$ for the five t -intervals as given in Table I (a) - (e). The asymmetry $\varepsilon'(\varphi)$ for the whole measured t -range (f). The red curves represent the best fit to Eq. (12) (a) - (e) and Eq. (13) (f).

V. SINGLE SPIN ASYMMETRIES

The azimuthal angle dependence of the cross-section for the elastic collision of vertically polarized protons is given [25] by:

$$\begin{aligned} \frac{d^2\sigma}{dt d\varphi} &= \frac{1}{2\pi} \frac{d\sigma}{dt} \cdot [1 + (\mathcal{P}_B + \mathcal{P}_Y)A_N(t)\cos\varphi \\ &\quad + \mathcal{P}_B\mathcal{P}_Y(A_{NN}(t)\cos^2\varphi + A_{SS}(t)\sin^2\varphi)], \end{aligned} \quad (11)$$

where higher order terms are ignored, $d\sigma/dt$ is the spin-averaged cross-section, \mathcal{P}_B and \mathcal{P}_Y are the beam polarizations for the two colliding beams (called Blue and Yellow). The double spin asymmetry A_{NN} is defined as the cross-section asymmetry for scattering of protons with spin orientations parallel and antiparallel with respect to the unit vector \hat{n} , normal to the scattering plane. The asymmetry A_{SS} is defined analogously for both beams fully polarized along the unit vector \hat{s} in the scattering plane and normal to the beam.

For each of the four RHIC stores, the event sample satisfying the requirements for elastic scattering was divided into five t -bins. Within each t -bin, the φ distributions were subdivided into bins of 10° . The raw asymmetry, $\varepsilon_N(\varphi)$, was calculated using geometric means [26], the so-called “square root formula” for each pair of φ and $\pi - \varphi$ bins in the range $-\pi/2 < \varphi < \pi/2$:

$$\varepsilon_N(\varphi) = \frac{(\mathcal{P}_B + \mathcal{P}_Y)A_N \cos(\varphi)}{1 + \nu(\varphi)} = \frac{\sqrt{N^{\uparrow\uparrow}(\varphi)N^{\downarrow\downarrow}(\pi - \varphi)} - \sqrt{N^{\downarrow\downarrow}(\varphi)N^{\uparrow\uparrow}(\pi - \varphi)}}{\sqrt{N^{\uparrow\uparrow}(\varphi)N^{\downarrow\downarrow}(\pi - \varphi)} + \sqrt{N^{\downarrow\downarrow}(\varphi)N^{\uparrow\uparrow}(\pi - \varphi)}}, \quad (12)$$

where the “ \uparrow ” and “ \downarrow ” indicate the spin direction of the transversely polarized colliding proton beam bunches, N is the number of events detected in the respective spin and respective φ states and $\nu(\varphi) = \mathcal{P}_B\mathcal{P}_Y(A_{NN}\cos^2(\varphi) + A_{SS}\sin^2(\varphi))$.

In the square root formula (12), the relative luminosities of different spin direction combinations cancel out. In addition, the detector acceptance and efficiency also cancel out, provided they do not depend on the bunch polarization. Results of Ref. [19] and preliminary results of this experiment [20] show that both A_{NN} and A_{SS} are very small ≈ 0.005 (and compatible with zero), constraining $\nu(\varphi)$ to ≈ 0.002 , which can be safely neglected.

For each RHIC store, the obtained raw asymmetries were divided by the sum of polarizations of both beams for this particular store, and then averaged over the stores. The resulting asymmetries for each t bin are shown in Fig. 3(a-e) as a function of φ . The solid lines represent the best fits to Eq. (12).

Along with the raw asymmetry, ε_N , which is proportional to the sum of the beam polarizations ($\mathcal{P}_B + \mathcal{P}_Y$), other asymmetries can be obtained using different combinations of bunch spin directions. For instance, the asymmetry proportional to the beam polarization difference ($\mathcal{P}_B - \mathcal{P}_Y$) is defined as follows:

$$\varepsilon'(\varphi) = \frac{(\mathcal{P}_B - \mathcal{P}_Y)A_N \cos(\varphi)}{1 - \nu(\varphi)} = \frac{\sqrt{N^{\uparrow\downarrow}(\varphi)N^{\downarrow\uparrow}(\pi - \varphi)} - \sqrt{N^{\downarrow\uparrow}(\varphi)N^{\uparrow\downarrow}(\pi - \varphi)}}{\sqrt{N^{\uparrow\downarrow}(\varphi)N^{\downarrow\uparrow}(\pi - \varphi)} + \sqrt{N^{\downarrow\uparrow}(\varphi)N^{\uparrow\downarrow}(\pi - \varphi)}}. \quad (13)$$

Provided that the beam polarizations (\mathcal{P}_B and \mathcal{P}_Y) have the same values, which is approximately valid in this experiment, one would expect $\varepsilon' = 0$. The derived values of ε' may be used to estimate false asymmetries, which remain after applying the ‘‘square root’’ method. The distribution of the asymmetry ε' , obtained for the whole t -range, together with its fit, is shown in Fig. 3(f).

During data taking, 64 bunches ($16\uparrow\uparrow$, $16\downarrow\downarrow$, $16\uparrow\downarrow$, $16\downarrow\uparrow$) of the 90 proton beam bunches collided with usable spin patterns, and were used for ε_N and ε' calculations.

The major systematic uncertainties of the experiment are due to the error of the beam polarization measurement, the reconstruction of t and a small background contribution as shown in Fig. 2. The two main contributions to the uncertainty in the t reconstruction are due to the uncertainties of the L^{eff} values and the position of the beam center at the RP location. The former is mostly due to the uncertainty on values of the magnetic field strength in the Q1-Q3 focusing quadrupoles, which is mainly due to uncertainties in the magnet current and field measurements. The correction to the strength was derived using the correlation between the angle and position in the RPs for the tracks in the regions where the detector acceptance overlaps. An overall correction to the strength of the focusing quadrupoles of 0.5% was applied. The residual systematic error of the field calculation was estimated to be $\approx 0.5\%$, leading to $\approx 1\%$ uncertainty in L^{eff} and $\approx 1.4\%$ uncertainty in t [27].

The position of the beam center is the reference point for the scattering angle calculations and effectively absorbs a large set of geometrical unknowns such as beam crossing angles and transverse beam positions at the IP, beam shifts from the beam pipe center at the RP location, as well as survey errors. To accommodate all these uncertainties, corrections to the survey were introduced based on the comparison of the simulated to the measured (x, y) distributions at the horizontal RPs on both sides of the IP. The simulation of the transport of elastically scattered protons through the RHIC magnets and the apertures was done and the detector acceptance was calculated. The acceptance boundaries from that simulation and the data were compared. No correction was found for the West side, while for the East side a correction of $(\Delta x, \Delta y) = (2.5, 1.5)$ mm was obtained. The uncertainty of that correction was estimated to be $400 \mu\text{m}$. After applying that alignment correction, the collinearity, defined as the average angle difference $\delta\theta_{x,y}$ (see Eq. (10)), was reduced from $\approx 55 \mu\text{rad}$ to $\approx 10 \mu\text{rad}$. The remaining alignment uncertainty leads to a value of $\delta t/t = 0.0020$ [GeV/c]/ \sqrt{t} and was added in quadrature to the uncertainty due to L^{eff} . The number of background events in the data is less than 1% in all t -bins (e.g. see Fig. 2). Assuming the background is beam polarization independent, the asymmetry will be diluted by the same amount, $\delta A_N/A_N < 0.01$. This value results in a negligible contribution to the total error, when statistical and systematic errors are added in quadrature.

The polarization values of the proton beams were determined by the RHIC CNI polarimeter group. Polarizations and their uncertainties (statistical and systematic combined) for the four stores were: 0.623 ± 0.052 , 0.548 ± 0.051 , 0.620 ± 0.053 , 0.619 ± 0.054 (Blue beam), 0.621 ± 0.071 , 0.590 ± 0.048 , 0.644 ± 0.051 , 0.618 ± 0.048 (Yellow beam) [28]. The overall luminosity-weighted average polarization values for all four stores are $\langle \mathcal{P}_B + \mathcal{P}_Y \rangle = 1.224 \pm 0.038$ and $\langle \mathcal{P}_B - \mathcal{P}_Y \rangle = -0.016 \pm 0.038$. Taking into account the overall uncertainty for normalization in polarization measurements, the total polarization error $\delta \langle \mathcal{P}_B + \mathcal{P}_Y \rangle / \langle \mathcal{P}_B + \mathcal{P}_Y \rangle$ is 5.4%.

If the false asymmetry ε_F were proportional to the beam polarization values, it would be indistinguishable from A_N . On the contrary, if it does not depend on the polarization, it contributes equally to both ε_N and ε' :

$$\varepsilon_N = A_N(\mathcal{P}_B + \mathcal{P}_Y) + \varepsilon_F, \quad (14)$$

$$\varepsilon' = A_N(\mathcal{P}_B - \mathcal{P}_Y) + \varepsilon_F. \quad (15)$$

and a direct estimate on the false asymmetry can be obtained:

$$\varepsilon_F = \frac{\varepsilon'(\mathcal{P}_B + \mathcal{P}_Y) - \varepsilon_N(\mathcal{P}_B - \mathcal{P}_Y)}{2\mathcal{P}_Y} \approx \varepsilon' - \varepsilon_N \frac{\mathcal{P}_B - \mathcal{P}_Y}{\mathcal{P}_B + \mathcal{P}_Y}. \quad (16)$$

The values of the raw asymmetries, measured in the whole t -range, are $\varepsilon_N = 0.0276 \pm 0.0004$ and $\varepsilon' = -0.0007 \pm 0.0004$. This gives a false asymmetry of $\varepsilon_F = -0.0004 \pm 0.0010$. Thus the conclusion is that the false asymmetry is consistent with zero and very small compared to the measured raw asymmetry ε_N .

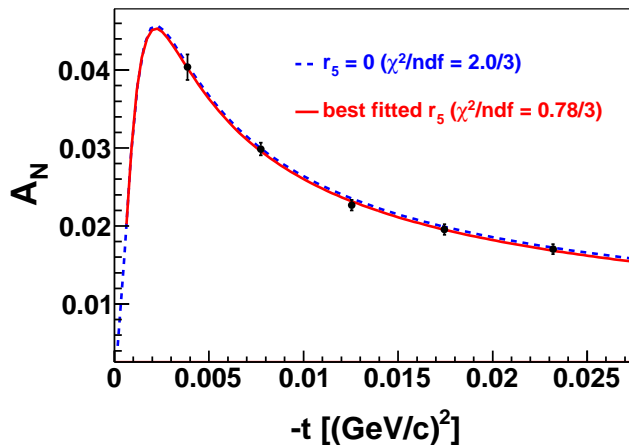


FIG. 4: (color online) The measured single spin asymmetry A_N for five $-t$ intervals. Vertical error bars show statistical uncertainties. Statistical error bars in $-t$ are smaller than the plot symbols. The dashed curve corresponds to theoretical calculations without hadronic spin-flip and the solid one represents the r_5 fit.

The results of the A_N measurements in the five t -bins are summarized in Table I together with associated uncertainties and $-t$ range boundaries. Two independent analyses of the data performed with slightly different selection criteria by two different groups gave consistent results. We have also done the cross checks to extract A_N using the beam polarizations of the two beams. The resulting A_N were found to be compatible with those in Table I within their statistical uncertainties.

$-t$ [(GeV/c) ²]	0.003 - 0.005	0.005 - 0.01	0.01 - 0.015	0.015 - 0.02	0.02 - 0.035
No. of Events	444045	2091977	2854764	2882893	2502703
$\langle -t \rangle$ [(GeV/c) ²]	0.0039	0.0077	0.0126	0.0175	0.0232
δt [(GeV/c) ²](syst.)	0.0001	0.0002	0.0003	0.0004	0.0004
A_N	0.0403	0.0299	0.0227	0.0196	0.0170
δA_N (stat.)	0.0016	0.0008	0.0007	0.0007	0.0007
δA_N (syst.)	0.0021	0.0016	0.0012	0.0010	0.0009

TABLE I: A_N values in five t ranges with associated uncertainties. Statistical errors for t are negligible and combined systematic errors are shown (See the text for details). Statistical errors and systematic errors on A_N are also shown, where δA_N (syst.) is a scale error due to the beam polarization.

VI. RESULTS AND CONCLUSIONS

The measured values of A_N are shown in Table I and presented in Fig. 4 together with parameterizations based on formula (5): the dashed line corresponds to no hadronic spin-flip contribution, i.e. $r_5 = 0$, while the solid line is the result of the fit using r_5 as a free parameter. Other parameter values used in the fit are: $\sigma_{\text{total}} = 51.79 \pm 0.12$ mb, $\rho = 0.1278 \pm 0.0015$ taken from fits to the world pp and p \bar{p} data [29, 30] and $B = 16.3 \pm 1.8$ (GeV/c)⁻² from Ref. [23].

The value of r_5 resulting from the fit described above is shown in Fig. 5 together with 1σ confidence level contours.

In Table II, we show the central value of the fit and uncertainties on $\text{Re } r_5$ and $\text{Im } r_5$ due to the listed effects. In the first row of the table, the statistical error to the fit with the central value of the parameters is shown. The remaining rows show changes of $\text{Re } r_5$ and $\text{Im } r_5$, when each parameter was varied one by one by $\pm 1\sigma$ during the fit procedure. Rows 2 and 3 show the effect due to the systematic uncertainty in L^{eff} and alignment, row 4 due to the beam polarization (vertical scale uncertainty of A_N) and rows 5-7 systematic contributions due to the uncertainty of fit parameters. The dominant source of the systematic uncertainty is due to the beam polarization uncertainty. The total systematic uncertainty, including the effects related to rows 2-7 of Table II, is obtained by adding the error covariance matrices.

The final result on r_5 is shown in Fig. 5 together with both statistical and systematic uncertainties. The obtained values $\text{Re } r_5 = 0.0017 \pm 0.0063$ and $\text{Im } r_5 = 0.007 \pm 0.057$ are consistent with the hypothesis of no hadronic spin-flip contribution at the energy of this experiment.

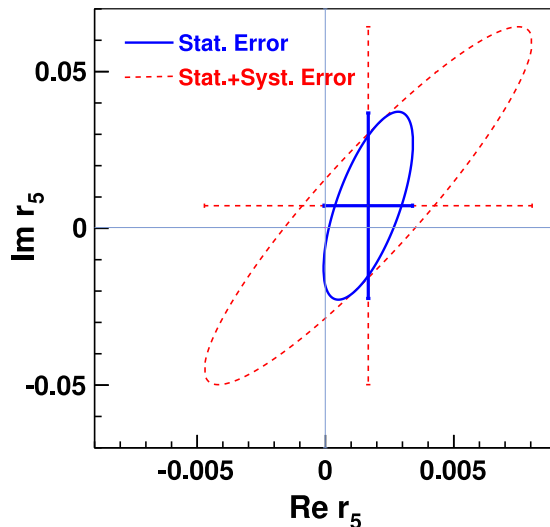


FIG. 5: (color online) Fitted value of r_5 with contours corresponding to statistical error only (solid ellipse and cross) and statistical+systematic errors (dashed ellipse and cross) of 1σ .

	central value	$\text{Re } r_5=0.0017$	$\text{Im } r_5=0.007$
	uncertainties	$\delta \text{Re } r_5$	$\delta \text{Im } r_5$
1	statistical	0.0017	0.030
2	$\delta t(L^{\text{eff}})$	0.0008	0.005
3	$\delta t(\text{alignment})$	0.0011	0.011
4	$\delta \mathcal{P}$	0.0059	0.047
5	$\delta \sigma_{\text{total}}$	0.0003	0.002
6	$\delta \rho$	< 0.0001	< 0.001
7	δB	< 0.0001	< 0.001
	total syst. error	0.0061	0.049
	total stat. + syst. error	0.0063	0.057

TABLE II: The fitted r_5 values including the uncertainties. (1): Statistical uncertainties. (2)-(4): Systematic uncertainties associated with this measurement. (5)-(7): Systematic uncertainties associated with the values used in the fit function. See the text for details.

Since the maximum A_N in the CNI region can be evaluated as $\kappa - 2\text{Im } r_5$ in Eq. (5), theoretical calculations emphasize values of $\text{Im } r_5$. Measurements of $\text{Im } r_5$ at different energies in the range $6.8 \text{ GeV} \leq \sqrt{s} \leq 200 \text{ GeV}$ are shown in Fig. 6, together with predictions of theoretical models of the hadronic spin-flip amplitude as discussed above. All of the experimental results, including that reported here, are consistent with the assumption of no hadronic spin-flip contribution to the elastic proton-proton scattering. The high accuracy of the current measurement provides strong limits on the size of any hadronic spin-flip amplitude at this high energy, hence significantly constraining theoretical models which require hadronic spin-flip.

Acknowledgments

We thank the RHIC Operations Group and RCF at BNL, the NERSC Center at LBNL and the Open Science Grid consortium for providing resources and support. This work was supported in part by the Offices of NP and HEP within the U.S. DOE Office of Science, the U.S. NSF, the Sloan Foundation, CNRS/IN2P3, FAPESP CNPq of Brazil, Ministry of Ed. and Sci. of the Russian Federation, NNSFC, CAS, MoST, and MoE of China, GA and MSMT of the Czech Republic, FOM and NWO of the Netherlands, DAE, DST, and CSIR of India, Polish Ministry of Sci. and Higher Ed., National Research Foundation (NRF-2012004024), Ministry of Sci., Ed. and Sports of the Rep. of

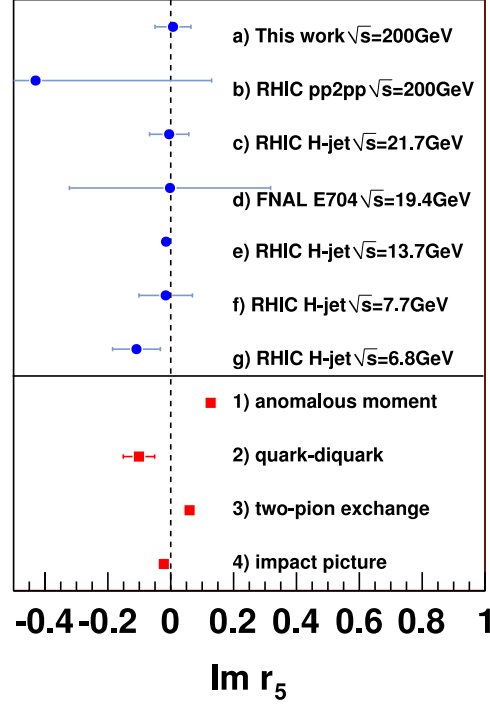


FIG. 6: (color online) Measurements of $\text{Im}(r_5)$ values for (a) this experiment, (b) RHIC pp2pp at $\sqrt{s}=200$ GeV [10], (c) RHIC H-jet target at $\sqrt{s}=21.7$ GeV [13], (d) FNAL E704 at $\sqrt{s}=19.4$ GeV [16], (e) RHIC H-jet target at $\sqrt{s}=13.7$ GeV [11], (f) RHIC H-jet target at $\sqrt{s}=7.7$ GeV [13], and (g) RHIC H-jet target at $\sqrt{s}=6.8$ GeV [12]. Theoretical calculations shown are (1) anomalous moment [7], (2) quark-diquark picture [8], (3) two-pion exchange model [5], and (4) impact picture [6]. The theoretical calculations are either energy independent (1,2,3) or done at $\sqrt{s}=200$ GeV (4). The vertical dashed line indicates where $\text{Im}(r_5)=0$. All error bars shown include both statistical and systematic errors.

Croatia, and RosAtom of Russia.

-
- [1] V. Barone, E. Predazzi, *High-Energy Particle Diffraction*, Texts and Monographs in Physics, Springer-Verlag; (2002), ISBN: 3540421076.
- [2] S. Donnachie, G. Dosch, P. Landshoff, *Pomeron Physics and QCD*, Cambridge University Press; (1998), ISBN: 9780521675703.
- [3] N. H. Buttimore *et al.*, Phys. Rev. **D59**, 114010 (1999).
- [4] T. L. Trueman, Phys. Rev. **D77**, 054005 (2008).
- [5] J. Pumplin and G. Kane, Phys. Rev. **D11**, 1183 (1975).
- [6] C. Bourrely, J. Soffer, and T.T. Wu, Phys. Rev. **D19**, 3249 (1979); Nucl. Phys. **B247**, 15 (1984).
- [7] M.G. Ryskin, Yad. Fiz. **46**, 611 (1987); Sov. J. Nucl. Phys. **46**, 337 (1987).
- [8] B.Z. Kopeliovich and B.G. Zakharov, Phys. Lett. **B226**, 156 (1989).
- [9] K. H. Ackermann *et al.*, Nucl. Instrum. Meth. **A 499**, 624 (2003).
- [10] S. Bültmann *et al.*, Phys. Lett. **B632**, 167 (2006).
- [11] H. Okada *et al.*, Phys. Lett. **B638**, 450 (2006).
- [12] I. G. Alekseev *et al.*, Phys. Rev. **D79**, 094014 (2009).
- [13] A. Bazilevsky *et al.*, Proceedings of SPIN 2010, J. Phys. Conf. Series. **295**, 012096 (2011).
- [14] O. Jinnouchi *et al.*, Proceedings of the 16th International Spin Physics Symposium *SPIN 2004*, eds. F. Bradamante *et al.*, World Scientific, (2005).
- [15] J. Tojo *et al.*, Phys. Rev. Lett. **89**, 052302 (2002).
- [16] N. Akchurin *et al.*, Phys. Rev. **D48**, 3026 (1993).
- [17] T.L. Trueman, Proceedings of the 16th International Spin Physics Symposium *SPIN 2004*, eds. F. Bradamante *et al.*, World

Scientific, (2005).

- [18] N. H. Buttmore *et al.*, Phys. Rev. **D18**, 694 (1978).
- [19] S. Bültmann *et al.*, Phys. Lett. **B647**, 98 (2007).
- [20] I.G. Alekseev for the STAR Collaboration, J. Phys. Conf. Ser. **295**, 012098 (2011).
- [21] T.L. Trueman, **arXiv:hep-ph/0604153**
- [22] S. Bültmann *et al.*, Nucl. Instr. Meth. **A535**, 415 (2004).
- [23] S. Bültmann *et al.*, Phys. Lett. **B579**, 245 (2004).
- [24] A. Drees, BNL Collider-Accelerator Department Note C-A/AP/441 (2012).
- [25] E. Leader, *Spin in Particle Physics*, Cambridge University Press (2001).
- [26] G.G. Ohlsen and P.W. Keaton Jr., Nucl. Instr. Meth. **109**, 41 (1973).
- [27] P. Pile *et al.*, Proceedings of 2012 International Particle Accelerator Conference (IPAC12), 2012, p. 1131.
- [28] CNI Polarimeter Group at BNL, <http://www.rhic.bnl.gov/~cnipol/pubdocs/Run09Offline>.
- [29] The COMPETE collaboration, <http://nuclth02.phys.ulg.ac.be/compete/predictor/>.
- [30] C. Bourrely *et al.*, Phys. Rev. **D76**,053002 (2007).